Hindawi
Journal of Electrical and Computer Engineering
Volume 2023, Article ID 9482825, 11 pages
https://doi.org/10.1155/2023/9482825

Research Article

A Novel Subspace Decomposition with Rotational Invariance Technique to Estimate Low-Frequency Oscillatory Modes of the Power Grid

Sudhansu Kumar Samal and Rajendra Kumar Khadanga

Department of Electrical and Electronics Engineering, Centurian University of Technology and Management, Odisha 752050, India

Correspondence should be addressed to Rajendra Kumar Khadanga; rajendrakhadanga@ieee.org

Received 18 December 2022; Revised 25 April 2023; Accepted 27 April 2023; Published 29 May 2023

Academic Editor: Jit S. Mandeep

This paper proposes modified Karhunen–Loeve transform with total least square estimation of signal parameters using rotational in-variance technique (MKLT-TLS-ESPRIT) to approximate the low-frequency oscillatory modes. MKLT decreases the impact of highly correlated additive colored Gaussian noise (ACGN) from the signal by differentiating the correlation matrix w.r.t from the final time instance. A quantitative study of the suggested method with other estimation methods is used to evaluate the effectiveness of the proposed method. Monte Carlo simulations with 50,000 runs are conducted to test the robustness of the estimation scheme for MKLT-TLS-ESPRIT. The evaluation of the efficiency of the proposed method in real-time perspective, the two-area system, and New England sixty-eight bus test system has been considered. The analysis shows that the suggested methodology correctly measures the interarea modes and lowers their mean and standard deviation to a minimum value.

1. Introduction

Wide-area integrated regional power networks are commonly affected by interarea oscillations (IAOs) when they are exposed to shedding of load, line loss, and fault. Such oscillations will lead to instability within the [1] interconnected networks. Small signal stability analysis (SSSA) utilizes state equations to approximate this IAOs by linearizing the power system. But, this technique suffers with heavy numerical burden, inconsistency in parameter estimation, and large computational time. Then, IAO modes need to be defined directly from the measured signal employing online techniques [2].

The use of measuring instruments, particularly wide area measurement systems (WAMSs), is drastically increased in the few last decades [3]. This allows higher precision IAOs estimates in both off and online. The online estimation methods are categorized as parametric and nonparametric approaches. Frequency estimation approaches, i.e., wavelet transform (WT) and continuous WT [4, 5] whose behavior is the same as a band-pass filter. In WT, changing the window size allows for multiresolution for both slow and fast frequency response. Multidimensional rotating frame measurements for synchronous machines during operations are available for mode estimation in [6]. Although WT can identify both long- and short-duration disturbances, its accuracy is dependent on the decomposition levels used and the mother wavelet used. There is currently no defined methodology for selecting the mother wavelet. Approaches addressed in the [7] like robust modified prony (RMP) and augmented prony (AP) [8] approximate the entire signal parameters by a provided sampled sequence, i.e., duration, direction, intensity, attenuation factor, and damping ratio. However, RMP and AP have a significant computing time problem, and AP does have a certain latency in large power system statistical analysis. Data-driven stochastic subspace identification (data-SSI) state space technique proposed in [9], which functions well under both ringdown and ambient

oscillations in power system. Since data-SSI concentrated on both estimation of the mode and selection of the model order, its computational time period is significant, which can contribute to the loss of synchronization. The authors of [10] proposed a new notch filtering approach along enhanced phase-locked loop to identify the damping factor. Another robust subspace, i.e., signal parameter estimation using rotational in-variance technique (ESPRIT) and its higher variants like modified TLS-ESPRIT [11, 12] are quite effective in terms of time-frequency resolution, fast computational time, and less sensitive to outliers. It is also possible to use the KLT-TLS-ESPRIT subspace-based technique [13], which is used for IAO dynamic phasor estimation.

This paper proposed an estimation method that fully denotes the signal as well as maximally compressed the information held by the signal. This proposed MKLT-TLS-ESPRIT technique can be extended to probing signals as well as for ringdown and ambient oscillations. It may work for small as well as huge power systems. The MKLT can be applied to estimate stationary as well as nonstationary signals.

For an efficient and precise measurement of the phase, the signal measured from a PMU must be held noise free. But because of the existence in outliers, the higher order harmonics, as well as unwanted spikes, get devolved in the signal. Employing a Hampel filter (HF), this spikes, and higher-order frequency components can be from a signal without smoothing the data. The remaining components of the noise are converted into highly correlated ACGN. Figure 1 describes the steps for MKLT implementation.

The contributions of the paper are as follows:

(i) The proposed technique effectively eliminates the influence of ACGN and compresses the information carried out by the signal maximally using samples decomposition onto a set of correlation matrix eigenvectors

(ii) Among various signal and noise subspace approaches presented over here, this proposed approach is more robust to outliers with the fastest computation

(iii) MKLT-TLS-ESPRIT performs more efficiently than the above methods when the signal strength buried with noise is very low or at SNRs 30 dB and 10 dB

(iv) The efficacy of the proposed approach for small and midsize power system is verified using IEEE benchmark two-area and IEEE sixteen-machine sixty-eight bus systems

(v) The proposed technique is evaluated under different complex conditions to check its robustness, such as the power system's unexpected detached load and three-phase short-circuit failure

The rest of the paper is structured according to the description. Section 2 discusses with the correct signal model the LFOs, also defines the impact of outliers in the power system, and also demonstrates the use of HF to eliminate outliers from the power signals. Section 3 discusses the use of MKLT-TLS-ESPRIT for estimation of inter-area mode. Section 4 sets out a step-by-step formulation of MKLT and TLS-ESPRIT for estimation of mode. Section 5 describes the results and discussions. Section 6 presents the functional applicability of the proposed technique using the IEEE benchmark two-area system. Section 7 includes the explanation of the efficacy of the proposed technique for IEEE sixteen-machine sixty-eight bus system, and the paper ends Section 8.

2. Problem Formulation for LFOs in Power System

The MKLT-TLS-ESPRIT proposed a new technique, which incorporates the [14] KL transformation theory and TLS-ESPRIT rotational invariance principles to estimate LFO modes.

2.1. Modeling of Power Grid Oscillations. The oscillations which address the dynamic conditions of the power grid represented using sinusoids which are exponentially damped. We called the active power, i.e., $r(n)$ flows in the IEEE benchmark two-area network tie-lines and also the IEEE sixteen-machine sixty-eight bus system. The oscillations from the power grid modeled are as follows:

$$r(n) = \sum_{k=1}^{K} \mathrm{a}_k e^{b_k n} \cos\left(n\omega_k + \phi_k\right). \tag{1}$$

Two deterministic quantities ($\{\omega_k\}$) and ($\{\mathrm{a}_k\}$) convey frequencies and amplitudes. The phases $\{\phi k\}$ are uncorrelated random variables, evenly spread over $(0, 2\pi)$, where attenuation component $\{\mathrm{b}_k\}$ and total sinusoid count K if the AWGN sequence, i.e., $w(n)$, influences the sinusoids, where $E[|w(n)|^2] = \sigma_\omega^2$ of zero mean and variance. The noise-component signal can be described as

$$R(n) = r(n) + w(n) = \sum_{j=1}^{L} \alpha_j e^{\beta_j n} + w(n), \tag{2}$$

where $\beta_j = b_j + i\omega_j$, $\alpha_j = (a_j/2)e^{i\phi_j}$, and $L = 2K$.

2.2. Effect of Outliers in Power System. The building of automated, interconnected regional electric power networks results generation of diverse and complex outlier data in the power system. Major causes of outlier are as follows:

(1) Signal acquisition capability: the limited potentiality of the sensors and WAMSs

(2) Power system failures: the power system failures such as transmission line outage and faults in the transmission lines

(3) Human influences: the involvement of the human in the signal measurement and control process may lead to the production of outlier data signal measurement

For a single out-of-scale measurement, the sample means of the estimation can be affected when the data sequence includes the outliers.

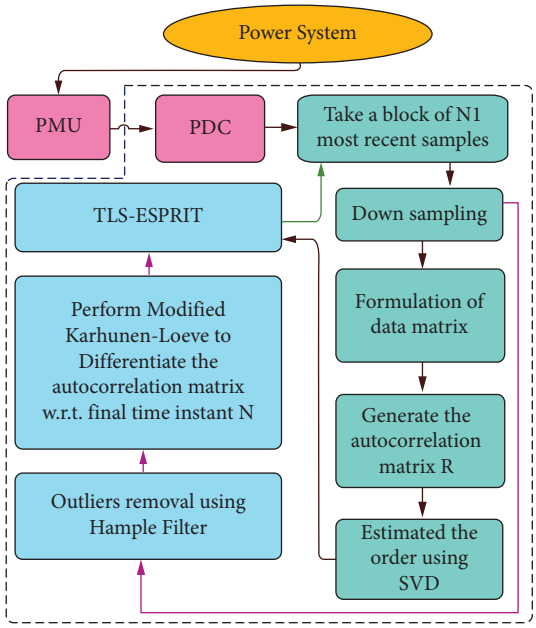

Figure 1: Steps for implementation of the proposed approach.

2.3. Removal of Outlier Using Hample Filter. The HF is a segment of the group of decision filters which uses the Hample identifier (HI) to remove the outliers from the input data sequence. The HI works on the principle of the three-sigma rule of statistics [15]. The width of the measurement window also plays a vital role outliers removal. The steps followed for the removal of outlier are described by the Algorithm 1.

3. Steps to Implement Proposed Approach to Estimate the Power Grid Oscillations

Let *N1* be the recent power measurements received from the tie-line using PMU. It can be expressed by a signal and noise vector using (2).

$$\mathbf{R}(n) = [R(n)R(n+1)\ldots R(n+M-1)]^T = \mathbf{r}(n) + \boldsymbol{\omega}(n), \tag{3}$$

where $\omega(n)$ and $\mathbf{r}(n)$ describe noise and signal vectors. Data matrix $(\mathbf{Y})$ can be constructed by using the vector $\mathbf{R}(n)$.

$$\mathbf{Y} = \left[\mathbf{R}^T(n)\right] = \begin{bmatrix} R(0) & R(1) & \cdots & R(M-1) \\ \vdots & \vdots & \vdots & \vdots \\ R(n) & R(n+1) & \cdots & R(n+M-1) \\ \vdots & \vdots & \vdots & \vdots \\ R(N-1) & R(N) & \cdots & R(N+M-2) \end{bmatrix}. \tag{4}$$

Signal vector $\mathbf{r}(n)$ can be descried using time-window frequency vector $\mathbf{V}$ given as follows:

$$\mathbf{R}(n) = \sum_{k=1}^{L} \alpha_k \mathrm{v}(f_k) e^{\beta_k n} + \mathbf{W}(n) = \mathbf{V}\boldsymbol{\Phi}^n\boldsymbol{\alpha} + \mathbf{W}(n), \tag{5}$$

where the time-window of length-M of the frequency vectors holds by the matrix $\mathbf{V}$ with L no. of columns.

$$\mathbf{V} = [\mathrm{v}(f_1)\,\mathrm{v}(f_2)\ldots\mathrm{v}(f_L)], \tag{6}$$

where $v(f) = [1\, e^{\beta_1} \ldots e^{(M-1)\beta_1}]$. α contains the complex sinusoid vectors α_k for $k = 1, 2, 3, \ldots, L\epsilon f_k$. The unitary diagonal matrix Φ having phase-shifts between the adjacent time samples of $\mathbf{R}(n)$ used to estimate the frequency given as follows:

$$\boldsymbol{\Phi} = \mathrm{diag}\left[e^{\beta_1} e^{\beta_2} \ \ldots \ e^{\beta_L}\right] = \mathrm{diag}[\phi_1, \phi_2, \ldots, \phi_L], \tag{7}$$

where $\phi_k = e^{\beta_k}$ for $k = 1,2,3, \ldots, L$.

The signal vector $\mathbf{r}(n)$ can be described with the sub-windowing process as $\mathbf{r}_{M-1}(n) = \mathbf{V}_{M-1}\Phi^n\alpha$.

The formulation of matrix $\mathbf{V}_{M-1}$ is similar as that of the $\mathbf{V}$. The matrix $\mathbf{V}_{M-1}$ can be represented as $v_{M-1}(f)$.

Using TLS-ESPRIT, the following matrices can be defined using $\mathbf{R}_{M-1}(n)$.

$$\mathbf{V}_1 = \mathbf{V}_{M-1}\boldsymbol{\Phi}^n \text{ and } \mathbf{V}_2 = \mathbf{V}_{M-1}\boldsymbol{\Phi}^{n+1}, \tag{8}$$

where unstaggered and staggered windows are expressed as $\mathbf{V}1$ and $\mathbf{V}2$. Frequency vectors of two subtime-window correlate as $\mathbf{V}_2 = \mathbf{V}_1\Phi$.

4. Application of Modified KLT for Interarea Oscillating Mode Estimation

The numerical code implementation of basic KLT approach [16, 17] is limited due to its larger computational burden and time. The idea behind the MKLT is to differentiate the "dominant eigenvalue" of the autocorrelation matrix with respect to the final instant "$\mathbf{N}$" of the basic KLT approach. The basic KLT approach fixes up the final time instant to $\mathbf{N} = 1$, which restricts the basic novelty of KLT that described by the finite, positive real $\mathbf{N}$ as a new continuous variable [12, 18].

Following steps need to be carried out to implement the modified KLT approach, i.e., the final variance of the projection coefficients.

Step 1 Consider the KLT of $\mathbf{R}(n)$ from (7) where $(0 < n < \mathbf{N})$.

$$\mathbf{R}(n) = \sum_{i=1}^{\infty} \mathbf{C}_i \Psi_i(n). \tag{9}$$

Step 2 First, using KLT the autocorrelation of sequence (9) can be expressed at different time instants, i.e.,

$$E\{\mathbf{R}(n_1)\mathbf{R}(n_2)\} = \sum_{j=1}^{\infty}\sum_{i=1}^{\infty} \Psi_j(n_1)\Psi_i(n_2)E\{\mathbf{C}_j\mathbf{C}_i\}. \tag{10}$$

Step 3 The independence property of the random variable $\mathbf{C}_i$, i.e., $E(\mathbf{C}_j\mathbf{C}_i) = \lambda_i\delta_{ji}$, where δ_{ji} denotes the Kronecker delta, defined as $\delta_{ji} = 0$ for $j \neq i$ and $\delta_{jj} = 1$, and λ_i is the new positive number sequence which is related to the variance of the corresponding random variable $\mathbf{C}_i$ as follows:

(1) Consider the $N1$ samples of signal $R(n)$ from (2).
(2) First, chose a moving window with odd length, which is composed of the current sample of the input signal and make the window centers around the current sample.
(3) Next, for the each current window data, its standard deviation σ_i and local median m_i would be computed.
$\text{medi an}\,(m_i) = \{R(i-l), R(i-l+1), \ldots, R_i, \ldots, R(i+l-1), R(i+l)\}$
$\text{StandardDeviation}\,(\sigma_i) = \kappa\times$
$\text{median}\,(|R(i-l)-m_i|, \ldots, |R(i+l)-m_i|)$
where κ is the scale factor which is given by $\kappa = 1/\sqrt{2}efrc1/2 \approx 1.4826$.
σ_i/k describes the median absolute deviation (MAD). For a normally distributed data, the scale factor (k) is equal to 1.4826, which makes the standard deviation estimate a unbiased for Gaussian data.
(4) Recent sample would be compared with $t_\sigma\sigma_i$, where threshold value is given by t_σ.
(5) If the filter identifies the current sample, P_i, then the HF replaces the median with current samples as follows:
$$y(i) = \begin{cases} R(i) | R(i) - m_i| \le t_\sigma\sigma_i \\ m_i | R(i) - m_i| > t_\sigma\sigma_i \end{cases}$$
With the increase of t, we can reduce the effect of HF over the signal. If t is 0, then the HF behaves as a regular median filter.

Algorithm 1: Steps for removal of outlier.

$$\sigma^2_{\mathbf{C}_i} = \lambda_i = E\left\{\mathbf{C}_i^2\right\} > 0. \tag{11}$$

Step 4 Using statistical orthogonal property of the random variable $\mathbf{C}_i$, i.e., $E(\mathbf{C}_j\mathbf{C}_i) = \lambda_i\delta_{ji}$ and taking the summation of both the time instant in one place, i.e., $i = j$, (10) reduced to

$$E\{\mathbf{R}(n_1)\mathbf{R}(n_2)\} = \sum_{j=1}^{\infty}\lambda_j\Psi_j(n_1)\Psi_j(n_2), \tag{12}$$

where $E(\mathbf{C}_j\mathbf{C}_i) = \lambda_i\delta_{jj}$.

Step 5 As the random function $R(n)$ has zero mean value in the finite time interval, we can replace the instant $n1 = n2 = n$ to get the variance from the autocorrelation and indexing it by i, and (12) can be expressed by referring (11)

$$E\left\{\mathbf{R}^2(n)\right\} = \sum_{i=1}^{\infty}\lambda_i\Psi_i^2(n). \tag{13}$$

Step 6 Using the property of orthogonality, $\Psi_i(n)$ should be normalized to one by integrating (13) on both sides with respect to n for 0 to $\mathbf{N}$

$$\int_0^{\mathbf{N}} E\left\{\mathbf{R}^2(n)\right\}dn = \sum_{i=1}^{\infty}\lambda_i\int_0^{\mathbf{N}}\Psi_i^2(n)\mathrm{d}n = \sum_{i=1}^{\infty}\lambda_i. \tag{14}$$

Step 7 For this given zero mean random process $\mathbf{R}(n)$, it can introduce the variance $\sigma^2_{\mathbf{R}(n)}$ of the $\mathbf{R}(n)$, i.e.,

$$\sigma^2_{\mathbf{R}(n)} = E\left\{\mathbf{R}^2(n)\right\} - E^2\{\mathbf{R}(n)\} = E\left\{\mathbf{R}^2(n)\right\}. \tag{15}$$

Substituting (15) into (14) gives

$$\int_0^{\mathbf{N}}\sigma^2_{\mathbf{R}(n)}\mathrm{d}n = \sum_{i=1}^{\infty}\lambda_i. \tag{16}$$

Step 8 (16) shows that the right side of the summation of eigenvalues λ_i must be the few functions of the final instant $\mathbf{N}$ as left side, i.e., $\lambda_i \equiv \lambda_i(\mathbf{N})$.

Step 9 Now, differentiating both side of (16) with respect to the final instant $\mathbf{N}$ yields

$$\sigma^2_{\mathbf{R}(\mathbf{N})} = \sum_{i=1}^{\infty}\frac{\partial\lambda_i(\mathbf{N})}{\partial\mathbf{N}}. \tag{17}$$

The above result $\sigma^2_{\mathbf{R}(\mathbf{N})}$ is called the final variance theorem. It shows that the final variance of any random stochastic process depends upon the final instant $\mathbf{N}$. Sum of the series of first-order partial derivatives for eigenvalues $\lambda_i(\mathbf{N})$ provides the final variance $\sigma^2_{\mathbf{R}(\mathbf{N})}$ with respect to the final instant $\mathbf{N}$.

4.1. Minimization of Complete Error by Utilizing Proposed MKLT-TLS-ESPRIT Technique. Algorithm 2 can be employed for estimation of modes by minimizing the total error between estimated subspace and actual signal subspace as suggested in [19].

5. Results and Discussion

The recent $N1$ samples provided by the PMU and phasor data concentrator (PDC) are considered for the IAO mode estimation using the proposed approach. The LFOs with nonlinearity may have approximately a stationary signal to achieve improved estimation. The MKLT-TLS-ESPRIT minimizes the SD and the bias of estimated modes. The approximation as an AWGN is regarded as a good analogy for modeling the measurement uncertainty received from the PMU's. However, some ACGN is detected in measurements because of the existence of an antialiasing filter (AAF) (with cut-off frequency between 400 and 1000 Hz) and signal processing algorithms that use convolution to estimate the phasors. At the performance, the ACGN is often ignored. A down-sampler then holds those quantities for further processing.

Additionally, a 10.24 s time window was used, referring to the PMU with the data rate of 512 samples (assuming data rate of 50 phasors/second). Usually, the variance in PMU

(1) Initially, signal vector $\mathbf{R}(n)$ from (3) is used to form a correlation matrix $R_{\mathbf{R}} \in \mathrm{R}^{N\times N}$.
(2) Defines MKLT of $\mathbf{R}(n)$ for a specified data matrix $\mathbf{Y}$ as $\mathbf{C}_i = \Psi^T\mathbf{Y}$
(3) Signal and noise subspaces can be obtained by disintegrating the $\underline{\Psi}_i$ i.e. $\underline{\Psi}_i = \left[\underline{\Psi}_{\mathrm{s}} \mid \underline{\Psi}_{\mathrm{n}}\right]$, where $\underline{\Psi}_{\mathrm{s}}$ represents signal subspace.
(4) The sub-space of the signal is then decomposed into two smaller subspaces (M-1) as dimension $\underline{\Psi}_{\mathrm{s}} = \begin{bmatrix} \underline{\Psi}_1 \\ * \quad * \quad * \quad * \end{bmatrix} = \begin{bmatrix} * \quad * \quad * \quad * \\ \underline{\Psi}_2 \end{bmatrix}$ where unstaggered and staggered subspaces, i.e., $\underline{\Psi}_1$ and $\underline{\Psi}_2$ describe in the same way as V_1 and V_2.
(5) These could be mapped as: $V_1 = \underline{\Psi}_1\mathrm{T}$ and $V_2 = \underline{\Psi}_2\mathrm{T}$. V_1 and V_2 are related as: $V_2 = V_1\Phi$ and $\underline{\Psi}_2 = \underline{\Psi}_1\Psi$ Substituting $\underline{\Psi}_2$ and V_1 in V_2 gives: $V_2 = \underline{\Psi}_2\mathrm{T} = \underline{\Psi}_1\Psi\mathrm{T}$ or $\mathrm{V}_2 = V_1\Phi = \underline{\Psi}_1\mathrm{T}\Phi$
(6) The correlation between both the subspaces provided by Algorithm 2 $\Psi\mathrm{T} = \mathrm{T}\Phi$ or $\Psi = \mathrm{T}\Phi\mathrm{T}^{-1}$
The Ψ eigenvalues are diagonal elements of Φ, where $\{\phi_k\}_{k=1,2,3\ldots L}$. T columns represent the eigenvectors of Ψ.
(7) Therefore, the frequency is given by $\widehat{f}_k = \angle\phi_k/2\pi$ where $\angle\phi_k$ is the phase of Φ_k.
(8) The TLS presents the exact response by minimizing the Frobenius norm of the $V_{1,2}$ true subspace and $\underline{\Psi}_{1,2}$ estimated subspace by reducing the errors $E_{1,2}$ [20] $\left\| E_1 \;\; E_2 \right\|_F$
(9) Compute the matrix $\widetilde{\Psi}$ of right singular vectors of $\left[\underline{\Psi}_1 \;\; \underline{\Psi}_2\right] = \widetilde{L}\widetilde{\Sigma}\widetilde{\Psi}^H$
(10) The matrix separation can be done using $\widetilde{\Psi} \in R^{2p\times 2p}$ in compliance with $\widetilde{\Psi} \in R^{p\times p}$ gives $\widetilde{\Psi} = \begin{bmatrix} \widetilde{\Psi}_{11} & \widetilde{\Psi}_{12} \\ \widetilde{\Psi}_{21} & \widetilde{\Psi}_{22} \end{bmatrix}$
(11) The singular values are computed using $\sigma_1, \sigma_2, \ldots, \sigma_M$ of the matrix $\Psi_{tls} = 0\widetilde{\Psi}_{12}\widetilde{\Psi}_{22}^{-1}$
(12) Algorithm 2 gives the frequency estimates using Algorithm 2.

Algorithm 2: Computational algorithm of TLS-ESPRIT.

measurements is assumed to be of 10^{-4} p.u. [21]. The North American SynchroPhasor Initiative (NASPI) offers standards for PMU and synchroPhasor measurements in different dynamic environments, such as energy variance 0.61×10^{-4} p.u.

5.1. Test Signal Corresponding to Interarea Mode. Simulations are conducted with a test signal having frequency = 0.4 Hz, magnitude = 1, and attenuationfactor = −0.07.

Figure 2 shows the effect of HF to above-mentioned test signal, i.e., interarea mode to minimize the outliers from the signal and final filtered signal further carried out for the process of frequency estimations. Figure 2(a) shows the signal with 10 dB, and Figure 2(b) 30 dB noise affected test signal and finally filtered out with less variance using HF.

A statistical comparison of the MKLT-TLS-ESPRIT, QR-TLS-ESPRIT, KLT-TLS-ESPRIT, RMP, and data-SSI for SNRs 10 dB and 30 dB is mentioned previously. The frequency and attenuation factor distribution of a test signal are shown in Figure 3. From Table 1, it is analyzed that the MKLT-TLS-ESPRIT method approximated the standard deviation and mean for the estimated frequency corresponding to interarea oscillating modes are 60.02% and 98.92%, respectively, of that obtained from the data-SSI approach and 60.51% and 99.47% for the KLT-TLS-ESPRIT approach with SNR 10 dB. It is also found that the standard deviation and mean of the estimated attenuation factor for the proposed MKLT-TLS-ESPRIT approach are approximately 76.99% and 54.93%, respectively, of that obtained in case of data-SSI and 63.12% and 70.31% for KLT-TLS-ESPRIT with SNR 10 dB. From Table 2, it is analyzed that the MKLT-TLS-ESPRIT method approximated that the standard deviation and mean for the estimated frequency corresponding to interarea oscillating modes are 59.68% and 99.4%, respectively, of that obtained in case of data-SSI and 55.02% and 99.67% for KLT-TLS-ESPRIT with SNR 30 dB. It is also found that the standard deviation and mean of the estimated attenuation factor for the MKLT-TLS-ESPRIT approach are approximately 56.6% and 88.53%, respectively, of that obtained in case of data-SSI and 36.31% and 78.03% for KLT-TLS-ESPRIT with SNR 30 dB.

5.2. Test Signal Corresponding to Local Area Mode. Simulation is conducted with a test signal having frequency = 1.5 Hz, maginitude = 1, and attenuationfactor = −0.1

Figure 4 shows the effect of HF to test signal, i.e., local-area mode to minimize the outliers of the signal and final filtered signal further carried out for the process of frequency estimations. Figure 4(a) shows the signal with 10 dB, and Figure 4(b) shows the signal with 30 dB noise affected test signal and finally filtered out with less variance using HF.

A statistical comparison of the MKLT-TLS-ESPRIT, QR-TLS-ESPRIT, KLT-TLS-ESPRIT, RMP, and data-SSI for SNRs 10 dB and 30 dB is mentioned as follows.

The frequency and attenuation factor distribution of a test signal are shown in Figure 5. From Table 3, it is analyzed that the MKLT-TLS-ESPRIT method approximated the standard deviation and mean for the estimated frequency corresponding to interarea oscillating modes are 46.29% and 99.81%, respectively, of the corresponding values obtained with data-SSI and 71.22% and 99.89% with KLT-TLS-ESPRIT for SNR 10 dB. It is also found that the standard deviation and mean of the estimated attenuation factor for the MKLT-TLS-ESPRIT approach are approximately 48.9% and 79.52%, respectively, of the obtained in case of data-SSI and 76.64% and 78.02% with ESPRIR + PM for SNR 10 dB. From Table 4, it is analyzed that the MKLT-TLS-ESPRIT method approximated that the standard deviation and mean for the estimated frequency corresponding to interarea oscillating modes are 61.21% and 99.80%, respectively, of the corresponding values obtained by applying data-SSI and 97.38% and 99.91% with KLT-TLS-ESPRIT for

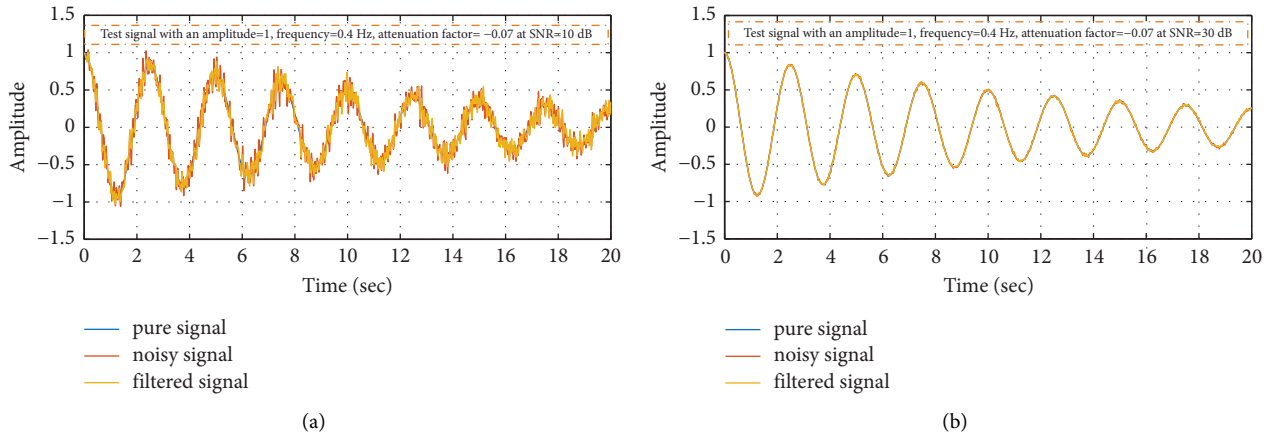

Figure 2: Test signals for interarea oscillating modes in power system using SNR 10 dB and 30 dB: (a) a test signal corresponds to interarea mode and (b) a test signal corresponds to interarea mode.

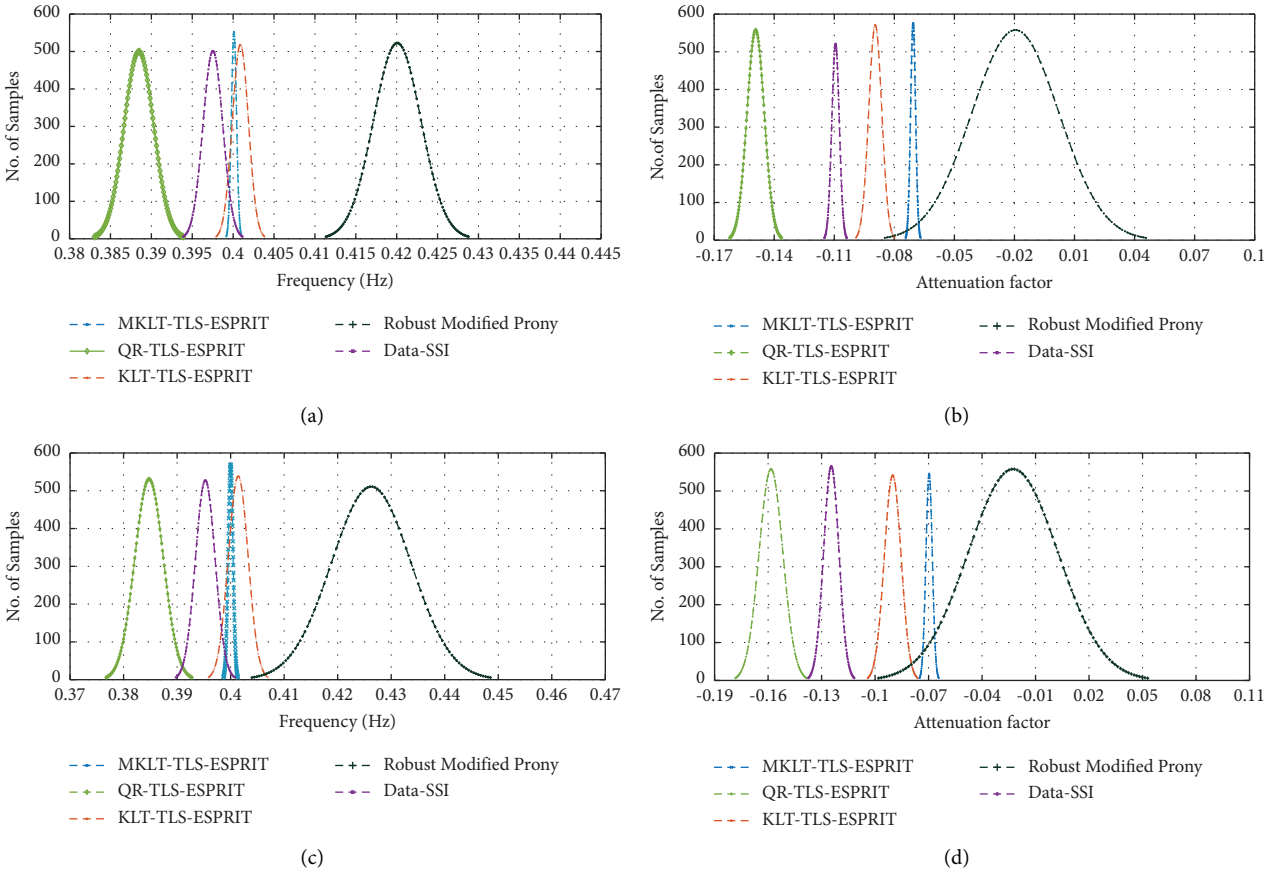

Figure 3: Interarea mode distribution utilizing Monte Carlo simulation at SNR 30 dB and 10 dB: (a) distribution of frequency using with SNR 30 dB, (b) distribution of attenuation factor using with SNR 30 dB, (c) distribution of frequency using with SNR 10 dB, and (d) distribution of attenuation factor using with SNR 10 dB.

SNR 30 dB. It is also found that the standard deviation and mean of the estimated attenuation factor for the MKLT-TLS-ESPRIT approach are approximately 19.06% and 91.50%, respectively, of that obtained in case of data-SSI and 59.88% and 79.74% with KLT-TLS-ESPRIT for SNR 30 dB.

5.3. Computational Time for Proposed MKLT-TLS-ESPRIT, QR-TLS-ESPRIT, KLT-TLS-ESPRIT, RMP, and Data-SSI. Figure 6 and Table 5 illustrate the comparison of the proposed MKLT-TLS-ESPRIT with QR-TLS-ESPRIT, RMP, data-SSI, and KLT-TLS-ESPRIT on the basis of their

Table 1: Statistical analysis for RMP, QR-TLS-ESPRIT, KLT-TLS-ESPRIT, data SSI, and MKLT-TLS-ESPRIT at SNR = 10 dB.

SNR = 10 dB	Frequency (Hz)			Attenuation factor		
	Std. dev.	Mean	Variance	Std. dev.	Mean	Variance
RMP	5.7577×10^{-3}	0.4289	3.3151×10^{-5}	1.6238×10^{-2}	−0.0216	2.6367×10^{-4}
QR-TLS-ESPRIT	1.4825×10^{-3}	0.3845	2.1978×10^{-6}	5.6437×10^{-3}	−0.1593	3.1851×10^{-5}
KLT-TLS-ESPRIT [12]	1.3823×10^{-3}	0.4022	1.9107×10^{-6}	3.3461×10^{-3}	−0.0997	1.1196×10^{-5}
Data-SSI	1.3893×10^{-3}	0.3958	7.7601×10^{-8}	2.7434×10^{-3}	−0.1276	7.5262×10^{-6}
MKLT-TLS-ESPRIT	8.3647×10^{-4}	0.4001	6.9968×10^{-7}	2.1123×10^{-3}	−0.0701	4.4618×10^{-6}

Table 2: Statistical analysis for RMP, QR-TLS-ESPRIT, KLT-TLS-ESPRIT, data-SSI, and MKLT-TLS-ESPRIT at SNR = 30 dB.

SNR = 30 dB	Frequency (Hz)			Attenuation factor		
	Std. dev.	Mean	Variance	Std. dev.	Mean	Variance
RMP	1.5286×10^{-3}	0.4201	2.3366×10^{-6}	1.3173×10^{-2}	−0.0201	1.7352×10^{-4}
QR-TLS-ESPRIT	1.2671×10^{-3}	0.3886	1.6055×10^{-6}	3.1347×10^{-3}	−0.1513	9.8263×10^{-6}
KLT-TLS-ESPRIT [12]	7.1862×10^{-4}	0.4013	5.8139×10^{-7}	3.1178×10^{-3}	−0.0897	9.7206×10^{-6}
Data-SSI	7.6249×10^{-4}	0.3976	5.8139×10^{-7}	2.3799×10^{-3}	−0.1173	5.6639×10^{-6}
MKLT-TLS-ESPRIT	3.9543×10^{-4}	0.4000	1.5636×10^{-7}	1.1322×10^{-3}	−0.0700	1.2818×10^{-6}

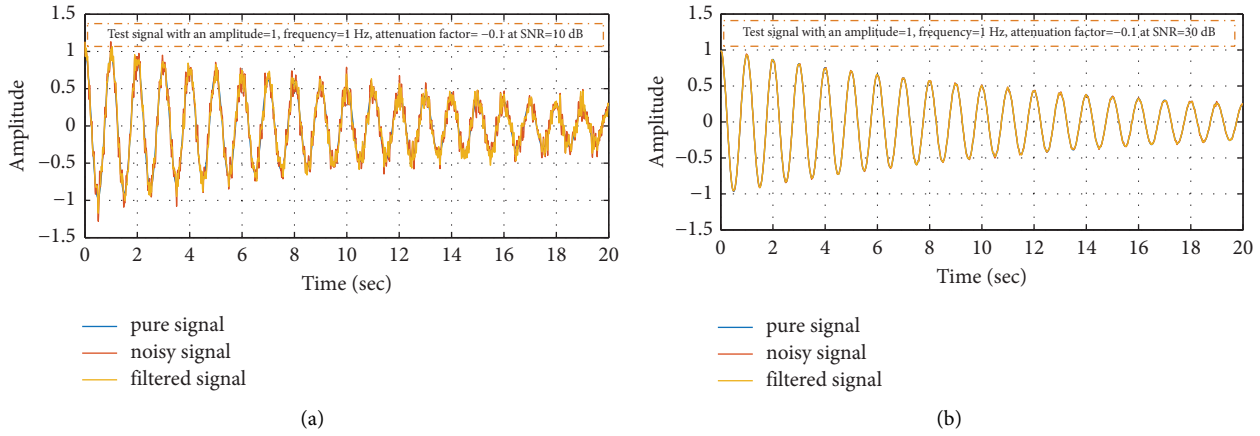

Figure 4: Test signals for local-area oscillating modes in power system using SNR 10 dB and 30 dB: (a) a test signal corresponds to local-area mode and (b) a test signal corresponds to local-area mode.

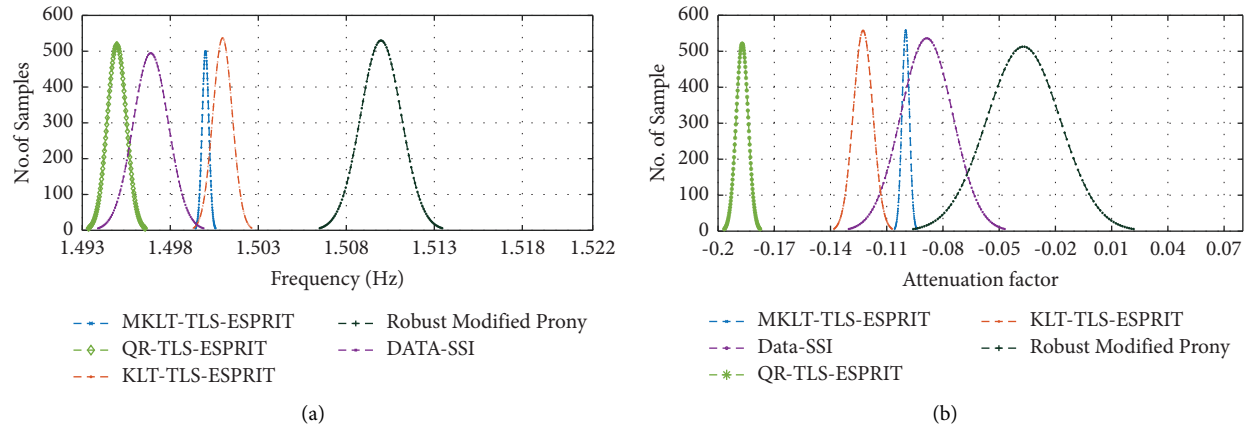

Figure 5: Continued.

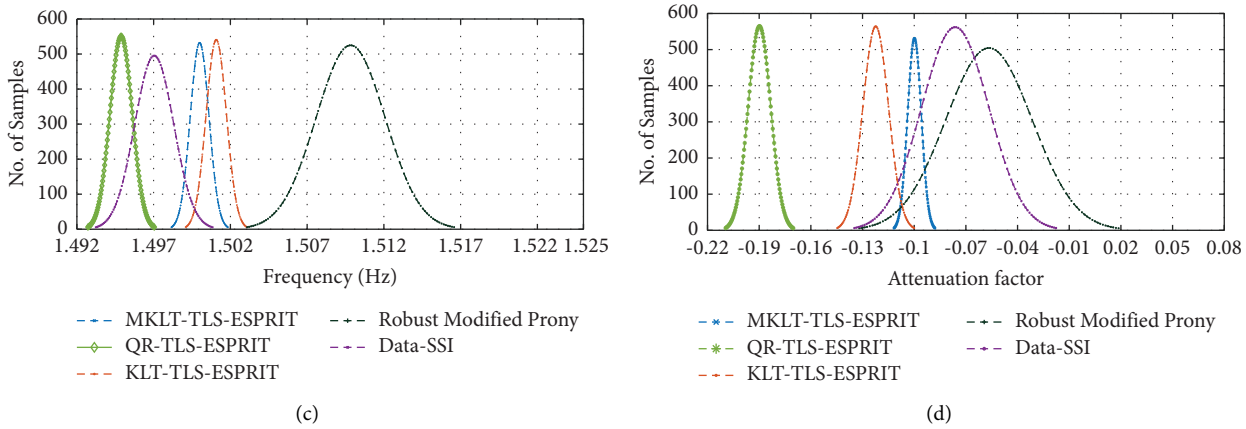

Figure 5: Local-area mode distribution utilizing 50,000 Monte Carlo simulation at SNR 30 dB and 10 dB: (a) distribution of frequency using with SNR 30 dB, (b) distribution of attenuation constant using with SNR 30 dB, (c) distribution of frequency using with SNR 10 dB, and (d) distribution of attenuation constant using with SNR 10 dB.

Table 3: Statistical analysis for RMP, QR-TLS-ESPRIT, KLT-TLS-ESPRIT, data-SSI, and MKLT-TLS-ESPRIT at SNR = 10 dB.

SNR = 10 dB	Frequency (Hz)			Attenuation factor		
	Std. dev.	Mean	Variance	Std. dev.	Mean	Variance
RMP	1.2267×10^{-2}	1.5105	1.5047×10^{-4}	1.5478×10^{-2}	−0.0547	2.3956×10^{-4}
QR-TLS-ESPRIT	5.0381×10^{-3}	1.4957	2.5382×10^{-5}	5.9367×10^{-3}	−0.1901	3.5244×10^{-5}
KLT-TLS-ESPRIT	5.4368×10^{-3}	1.5017	2.9558×10^{-5}	6.3465×10^{-3}	−0.1283	4.0278×10^{-5}
Data-SSI	8.3643×10^{-3}	1.4973	6.9961×10^{-5}	9.9432×10^{-3}	−0.0796	9.8867×10^{-5}
MKLT-TLS-ESPRIT	3.8721×10^{-3}	1.5001	1.4993×10^{-5}	4.8643×10^{-3}	−0.1001	2.3661×10^{-5}

Table 4: Statistical analysis for RMP, QR-TLS-ESPRIT, KLT-TLS-ESPRIT, data-SSI, and MKLT-TLS-ESPRIT at SNR = 30 dB.

SNR = 30 dB	Frequency (Hz)			Attenuation factor		
	Std. dev.	Mean	Variance	Std. dev.	Mean	Variance
RMP	9.7643×10^{-4}	1.5098	9.5341×10^{-7}	1.0328×10^{-2}	−0.0403	1.0667×10^{-4}
QR-TLS-ESPRIT	6.1631×10^{-4}	1.4951	3.7983×10^{-7}	2.8643×10^{-3}	−0.1914	8.2042×10^{-6}
KLT-TLS-ESPRIT	6.0531×10^{-4}	1.5014	3.6640×10^{-7}	3.6481×10^{-3}	−0.1254	1.3308×10^{-5}
Data-SSI	9.6289×10^{-4}	1.4971	5.8200×10^{-7}	1.1462×10^{-2}	−0.0915	1.3137×10^{-4}
MKLT-TLS-ESPRIT	5.8947×10^{-4}	1.5001	3.4747×10^{-7}	2.1847×10^{-3}	−0.1000	4.7729×10^{-6}

computational time used for IAO modes estimation. It is observed that for 2000 Monte Carlo simulation, the mean computational time taken by the MKLT-TLS-ESPRIT is 0.00501 sec for SNR = 30 dB and 0.00507 sec for SNR = 10 dB, whereas for the data-SSI is 0.0064 sec for SNR = 30 dB and 0.0067 sec for SNR = 10 dB. All tests are performed using Intel(R) Core(TM) i7-4790S CPU @ 3.20 GHz processor with 8 Gb RAM.

5.4. Variance Response to Different SNRs Using Proposed MKLT-TLS-ESPRIT, KLT-TLS-ESPRIT, RMP, and Data-SSI. Due to the accurate estimation of the signal frequency, variances of the data-SSI and MKLT-TLS-ESPRIT estimates are somewhat less than the ones for the two different estimates. Figure 7 shows that, for low SNRs, this process well predictable, where the variation by the estimation accuracy is less as compared to the variance by the noise.

6. LFO Modes Estimation for IEEE Benchmark Two-Area Grid System Using Proposed Algorithm

Figure 8 illustrates a test system [22] refers to IEEE benchmark two-area grid system. It includes two different areas, each are having two synchronous machines connected through eleven buses, via bus_7 and bus_9. There are three loads applied to the bus_7, bus_8, and bus_9 of the test system. There are also two shunt condensers mounted at bus_7 and bus_9. The test system operates with fundamental frequency of 60 Hz.

Case 1. IAO mode estimation using data from IEEE benchmark two-area grid system for tie-line short-circuit fault.

Employing the SSSA, the IAO modes of the power system are analyzed. For a period of 1.2 seconds, starting at

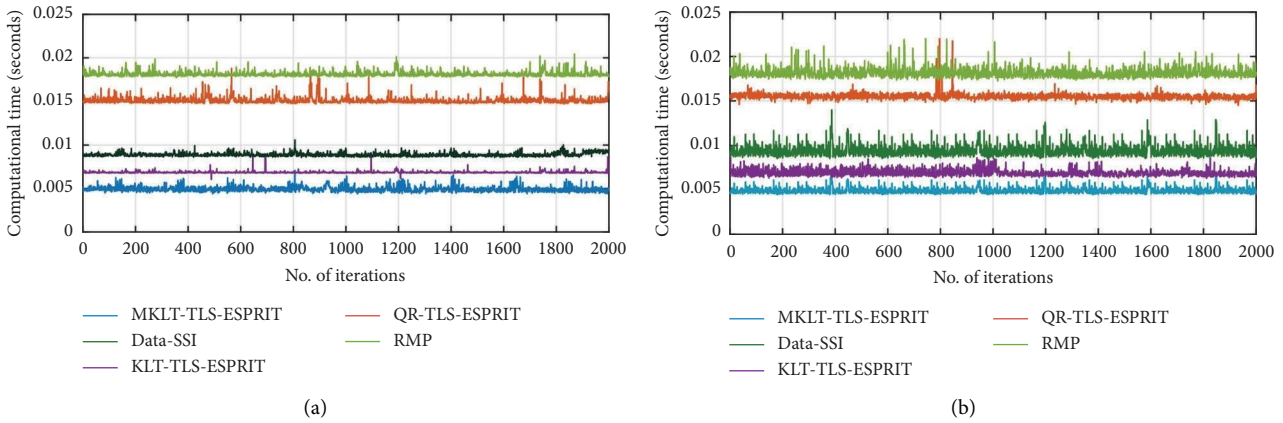

Figure 6: Computational time for different estimation algorithm: (a) computational time with SNR 30 dB and (b) computational time with SNR 10 dB.

Table 5: Computational time for RMP, QR-TLS-ESPRIT, KLT-TLS-ESPRIT, data-SSI, and proposed MKLT-TLS-ESPRIT at different SNRs.

Estimation algorithms	Computational time (sec)	
	SNR = 30 dB	SNR = 10 dB
RMP	0.0089	0.0091
QR-TLS-ESPRIT	0.0185	0.0189
KLT-TLS-ESPRIT	0.01561	0.01593
Data-SSI	0.0064	0.0067
MKLT-TLS-ESPRIT	0.00501	0.00507

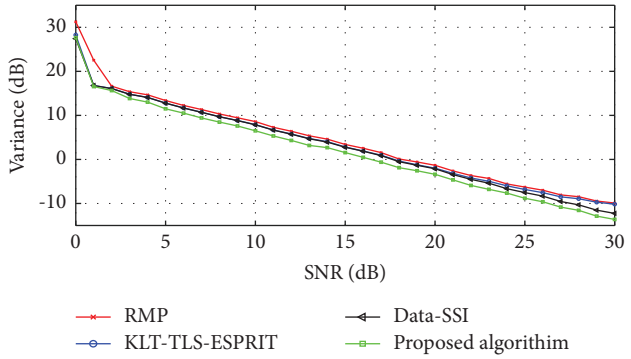

Figure 7: Variance comparison using proposed approach.

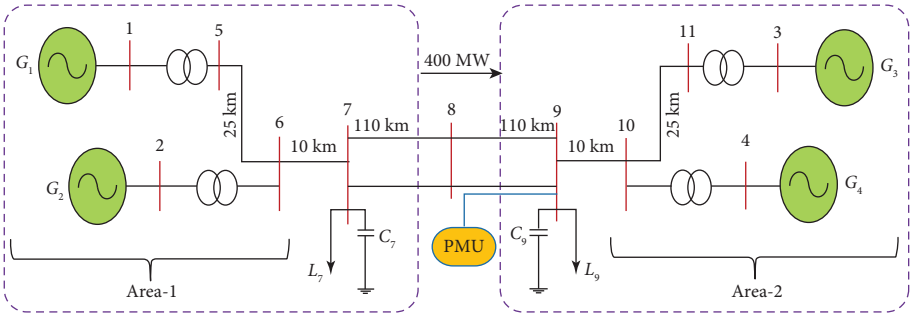

Figure 8: Schematic diagram of IEEE benchmark two-area grid system.

Table 6: Statistical analysis of the IAOs for IEEE benchmark two-area grid system with three-phase line short-circuit fault using RMP, QR-TLS-ESPRIT, KLT-TLS-ESPRIT, data-SSI, and MKLT-TLS-ESPRIT at SNR = 30 dB.

SNR = 30 dB	Frequency = 0.6366 Hz			Attenuation factor = −0.25		
	Std. dev.	Mean	Variance	Std. dev.	Mean	Variance
RMP	8.8334×10^{-4}	0.6229	7.1122×10^{-7}	7.3275×10^{-3}	−0.2120	5.369×10^{-5}
QR-TLS-ESPRIT	8.4935×10^{-4}	0.6138	7.2139×10^{-7}	2.5488×10^{-2}	−0.2257	6.4963×10^{-4}
KLT-TLS-ESPRIT	5.1392×10^{-4}	0.6373	1.2977×10^{-6}	8.9327×10^{-3}	−0.2143	7.9793×10^{-3}
Data-SSI	8.1013×10^{-4}	0.63893	6.5631×10^{-7}	8.9487×10^{-3}	−0.2293	8.0079×10^{-5}
MKLT-TLS-ESPRIT	3.4867×10^{-4}	0.63728	1.2157×10^{-7}	4.1550×10^{-3}	−0.2364	1.7264×10^{-5}

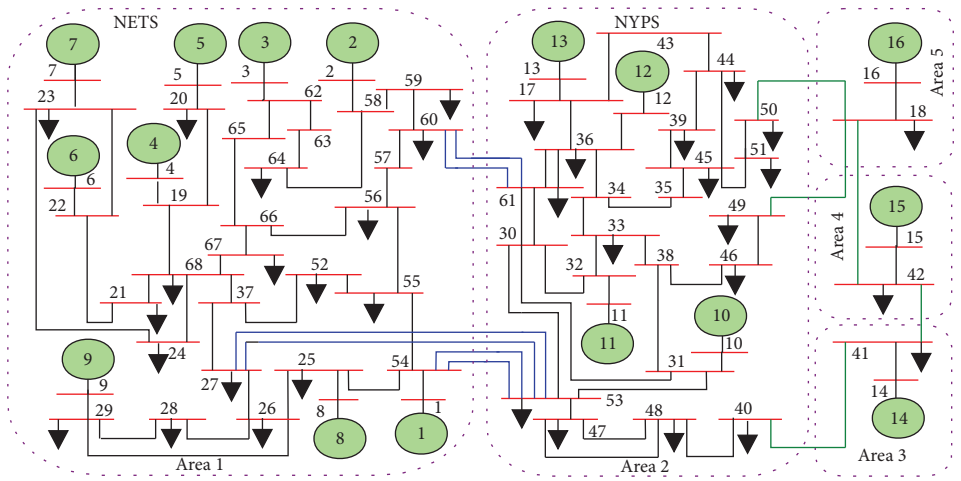

Figure 9: One line diagram of the 16-generator Sixty-Eight bus test system.

Table 7: Statistical analysis of the IAOs for sixteen-machine sixty-eight bus IEEE system using MKLT-TLS-ESPRIT at SNR = 30 dB.

SNR = 30 dB	Frequency (Hz)			Attenuation factor		
	True	Mean	Std. dev.	True	Mean	Std. dev.
Mode-1	0.3893	0.3899	0.00018	−0.1200	−0.1339	0.0039
Mode-2	0.5160	0.4971	0.00013	−0.2100	−0.2104	0.0041
Mode-3	0.5893	0.6693	0.00018	−0.1900	−0.1976	0.0054
Mode-4	0.7923	0.7804	0.00015	−0.2300	−0.2187	0.0017

1 second, a disturbance is provided by applying a short-circuit fault of three phases at tie-line close to bus_8. Figure 8 shows the real power flow between lines 10 and 9 provided by the PMU located at bus_9. The statistical SD, mean, and variance of the IAO modes extracted using Monte Carlo simulation for 50,000 runs are shown in Table 6. The SD calculated to express the statistical difference of the estimated attenuation factor and frequency from the actual SSSA using MKLT-TLS-ESPRIT by adding a noise of SNR 30 dB is given as 4.155×10^{-3} and 3.4867×10^{-4}. The statistical mean extracted by proposed MKLT-TLS-ESPRIT technique related to IAO mode, i.e., 0.6328 Hz, is nearly same that of the obtained in case of SSSA.

7. LFO Modes Estimation for IEEE Sixteen-Machine, Sixty-Eight Bus Test System Using Proposed Algorithm

Figure 9 shows the IEEE benchmark sixteen-machine sixty-eight bus grid system is considered to verify the efficacy of the proposed approach. This system's detailed parameter is listed within [23].

The grid comprised of five different areas: Area[1] and Area[2] with generators (Gen1 − Gen9) and (Gen10 − Gen13), Area(3), Area[4], and Area[5] comprise with generators (Gen14), (Gen15), and (Gen16). Different IAOs modes occurred in this power grid evaluated using SSSA are $M(1)$, $M(2)$, $M(3)$, and $M(4)$. Generators of Area[1] and Area[2] oscillates toward generators in Area[3], Area[4], and Area[5] with 0.3893 Hz correspond to $M(1)$. Generators of Area[1], Area[3], and Area[4] oscillate against the generators of Area[5] and Area[2] at 0.5166 Hz corresponds to $M(2)$. Generators of Area[1], Area[4], and Area(5) swing against generators of Area[2] and Area[3] at frequency 0.5893 Hz corresponds to $M(3)$. Generator in Area[4] oscillates against generators in Area[3] and Area[5] at the frequency of 0.7923 Hz corresponds to $M(4)$.

The statistical behavior of MKLT-TLS-ESPRIT is described in Table 7 using 2000 Monte Carlo runs, i.e., the SD of the estimated frequency and AF is given as (Freq.Std.) and (Attn.fact.-Std), the mean of the Frequency and the AF is given as (Freq mean), and the mean of the frequency and the AF is given as (F (Attn.factor.-mean). The IAO mode

calculated using MKLT-TLS-ESPRIT is found to be similar to the values corresponding to those measured using SSSA.

8. Conclusion

In this paper, we proposed a new interarea mode estimation approach based on subspace decomposition, to estimate the power system's IAO modes. The proposed estimation scheme of the IAOs is found to be more robust and also provides a precise mode estimation when the estimates are slightly affected by the highly correlated ACGN. It has also been examined that the MKLT-TLS-ESPRIT has improved estimation efficiency in reference to the QR-TLS-ESPRIT, RMP, KLT-TLS-ESPRIT, and data-SSI in aspects of standard deviation, variance, and the mean of the estimated IAO modes for given frequency and attenuation factor. Moreover, on IEEE benchmark two-area grid system and IEEE sixteen-machine sixty-eight bus system, the estimated performance of the proposed technique is evaluated. The performance of the MKLT-TLS-ESPRIT at SNR 30 dB with a case of short-circuit failure in three-phase line is analyzed. The observations made using the MKLT-TLS-ESPRIT technique is much similar to the estimated results obtained with SSSA.

Data Availability

The data supporting the current study are available from the corresponding author upon request.

Conflicts of Interest

The authors declare that they have no conflicts of interest.

References

[1] Y. X. Ni, S. S. Chen, and B. L. Zhang, *Theory and Analysis of Dynamic Power System*, Tsinghua University Press, Beijing, China, 2002.

[2] K. El-Naggar, "On-line measurement of low-frequency oscillations in power systems," *Measurement*, vol. 42, no. 5, pp. 716–721, 2009.

[3] Y. Wang and J. P. Hespanha, "Distributed estimation of power system oscillation modes under attacks on gps clocks," *IEEE Transactions on Instrumentation and Measurement*, vol. 67, no. 7, pp. 1626–1637, 2018.

[4] R. Janeliukstis, "Continuous wavelet transform-based method for enhancing estimation of wind turbine blade natural frequencies and damping for machine learning purposes," *Measurement*, vol. 172, Article ID 108897, 2021.

[5] U. Singh and S. N. Singh, "Application of fractional fourier transform for classification of power quality disturbances," *IET Science, Measurement and Technology*, vol. 11, no. 1, pp. 67–76, 2017.

[6] N. H. Chandra and A. Sekhar, "Wavelet transform based estimation of modal parameters of rotors during operation," *Measurement*, vol. 130, pp. 264–278, 2018.

[7] X. Xia, C. Li, and W. Ni, "Dominant low-frequency oscillation modes tracking and parameter optimisation of electrical power system using modified prony method," *IET Generation, Transmission and Distribution*, vol. 11, no. 17, pp. 4358–4364, 2017.

[8] M. Khodadadi Arpanahi, M. Kordi, R. Torkzadeh, H. Haes Alhelou, and P. Siano, "An augmented prony method for power system oscillation analysis using synchrophasor data," *Energies*, vol. 12, no. 7, p. 1267, 2019.

[9] T. Jiang, Y. Mu, H. Jia et al., "A novel dominant mode estimation method for analyzing inter-area oscillation in China southern power grid," *IEEE Transactions on Smart Grid*, vol. 7, no. 5, pp. 2549–2560, 2016.

[10] H. Zamani, M. Karimi-Ghartemani, and M. Mojiri, "Analysis of power system oscillations from pmu data using an epll-based approach," *IEEE Transactions on Instrumentation and Measurement*, vol. 67, no. 2, pp. 307–316, 2018.

[11] P. Tripathy, S. Srivastava, and S. Singh, "A modified tls-esprit-based method for low-frequency mode identification in power systems utilizing synchrophasor measurements," *IEEE Transactions on Power Systems*, vol. 26, no. 2, pp. 719–727, 2011.

[12] S. K. Samal and B. Subudhi, "New signal subspace approach to estimate the inter-area oscillatory modes in power system using tls-esprit algorithm," *IET Generation, Transmission & Distribution*, vol. 13, no. 18, pp. 4123–4140, 2019.

[13] P. Banerjee and S. Srivastava, "A subspace-based dynamic phasor estimator for synchrophasor application," *IEEE Transactions on Instrumentation and Measurement*, vol. 61, no. 9, pp. 2436–2445, 2012.

[14] C. Maccone, "The klt (karhunen–loève transform) to extend seti searches to broad-band and extremely feeble signals," *Acta Astronautica*, vol. 67, no. 11-12, pp. 1427–1439, 2010.

[15] F. R. Hampel, "The influence curve and its role in robust estimation," *Journal of the American Statistical Association*, vol. 69, no. 346, pp. 383–393, 1974.

[16] M. Najim, *Modeling, Estimation and Optimal Filtering in Signal Processing*, Wiley Online Library, Hoboken, NJ, USA, 2008.

[17] M. Lara and B. Mulgrew, "Performance of the distributed klt and its approximate implementation," in *Proceedings of the 2012 20th European Signal Processing Conference (EUSIPCO)*, pp. 724–728, IEEE, Bucharest, Romania, August, 2012.

[18] C. Maccone, *Mathematical SETI: Statistics, Signal Processing, Space Missions*, Springer Science & Business Media, Berlin, Germany, 2012.

[19] B. Subudhi, S. K. Samal, and S. Ghosh, "A new low-frequency oscillatory modes estimation using tls-esprit and least mean squares sign-data (lmssd) adaptive filtering," in *Proceedings of the Region 10 Conference, TENCON 2017-2017 IEEE*, pp. 751–756, IEEE, Penang, Malaysia, November. 2017.

[20] G. H. Golub and C. F. Van Loan, *Matrix Computations*, Vol. 3, JHU Press, Baltimore, ML, USA, 2012.

[21] K. E. Martin, "Synchrophasor standards and guides for the smart grid," in *Proceedings of the 2013 IEEE Power & Energy Society General Meeting*, pp. 1–5, IEEE, Vancouver, Canada, July, 2013.

[22] P. Kundur, N. J. Balu, and M. G. Lauby, *Power System Stability and Control*, Vol. 7, McGraw-Hill, New York, NY, USA, 1994.

[23] A. Singh and B. Pal, *New England 68-Bus Test System*, Texas A&M University Engineering, College Station, TX, USA, 2013.